Hindawi
International Journal of Photoenergy
Volume 2019, Article ID 1263480, 8 pages
https://doi.org/10.1155/2019/1263480

Research Article

Line-End Voltage and Voltage Profile along Power Distribution Line with Large-Power Photovoltaic Generation System

Toshiro Matsumura,[1] **Masumi Tsukamoto**,[1] **Akihiro Tsusaka**,[1] **Kazuto Yukita**,[1] **Yasuyuki Goto**,[1] **Yasunobu Yokomizu**,[2] **Kento Tatewaki**,[2] **Daisuke Iioka**,[3] **Hirotaka Shimizu**,[4] **Yuuki Kanazawa**,[5] **Hiroyuki Ishikawa**,[5] **Akimori Matsuo**,[5] **and Hideki Iwatsuki**[5]

[1]*Department of Electrical Engineering, Aichi Institute of Technology, Japan*
[2]*Nagoya University, Japan*
[3]*Tohoku University, Japan*
[4]*Polytechnic University, Japan*
[5]*Chubu Electric Power Co. Inc., Japan*

Correspondence should be addressed to Toshiro Matsumura; matukaze@aitech.ac.jp

Received 6 December 2018; Accepted 6 February 2019; Published 24 March 2019

Guest Editor: Marialaura Di Somma

In recent years, the introduction of the photovoltaic generation system (PV system) has been increasing by promoting the use of renewable energy. It has been feared that the reverse current from the PV system may cause an unacceptable level of voltage rise at the interconnection node in the power distribution system. This paper discusses the effects of the reverse current on the voltage rise and fall characteristics of the interconnection node and the voltage profiles along the power distribution line. When the line current on the circuit is small, the voltage on the line monotonically increases from the sending end to the receiving end. When a relatively large current flows, it causes a voltage reduction near the distribution substation. Furthermore, on the basis of the voltage aspects in the power distribution system with a large PV system, the allowable limits of the line current and the output power from PV system are investigated.

1. Introduction

In recent years, photovoltaic power generation systems (PV systems) have been encouraged and its introduction into the electric power distribution systems is being advanced as a matter of national policy in Japan. Numerous studies on the influence of interconnecting large PV systems on the power quality of the electrical power system have been performed [1–5]. It has been feared that a rise in voltage may be caused by the reverse current from the PV system in the power distribution system [6].

In general, the voltage rise due to the PV system in a distribution system is expressed by the magnitude of a reverse power flow. Several investigations have been conducted on the method of voltage regulation in a distribution system with a PV system. There has been growing recognition that the reactive power control of a PV system is useful in compensating for the voltage fluctuation which results from solar irradiance conditions [7]. The power factor control for distributed generation in a distribution network has been proposed to mitigate the voltage rise due to the active power output from the distributed generation [8]. It was suggested that the magnitude of reactive power injection from a PV system connected to a low-voltage grid was determined by the voltage sensitivity matrix [9]. A static var compensator (SVC) installed in a low-voltage distribution network has been proposed for suppressing the voltage rise due to the reverse power flow from the PV system [10]. A voltage regulator with a tap changer is also useful as a countermeasure against the voltage rise in the distribution

system. It was proposed that multiple line drop compensations controlled the tap position of a load tap changer in the distribution substation for the purpose of voltage regulation [11]. An online control strategy for the tap position has been proposed by using the measurement data of voltage, power, and tap position and the state estimation for the purpose of minimizing the number of tap operations [12].

On the contrary, the voltage reduction in a distribution feeder due to the reverse power flow from large-scale PV systems has been reported [13, 14]. As mentioned above, it is well accepted that the reverse power flow from a PV system causes the voltage rise in a distribution system. In [13, 14], the authors indicated that the voltage in a distribution feeder decreased with the increase in the reverse power flow from the PV system in cases where the reverse power flow is drastically larger than the supply power to the load in the distribution system. We showed from basic circuit theory that the large reverse current from a PV system might cause a reduction in the voltage of the interconnection node in the case of a long distribution line [15]. We also qualitatively and quantitatively indicated the effects of the distribution line length on the voltage rise and fall characteristics at the interconnection node [15].

This paper discusses the effects of a reverse current on the voltage rise and fall characteristics at the interconnection node and the voltage profiles along a power distribution line. Furthermore, the allowable limits of the line current and the output power are investigated on the basis of the voltage behavior in the power distribution system.

2. Distribution System Model

Figure 1 shows a single-phase equivalent circuit of a power distribution system with a large PV system at the receiving end. It is supposed that the distribution substation (sending end) voltage is $V_s = 6.6\,\text{kV}$, the line impedance per unit length is $r + jx$, and the reverse line current is $\boldsymbol{I}$. The total line impedance is $(r + jx)D$ for the whole line length of D.

In Japan, after the introduction of the Feed-in Tariff (FIT) scheme in 2012, large capacities of photovoltaic generators (PV) have been constructed in rural areas. These rural areas are relatively far from load centers where substations are located, and so, large capacities of PV are connected near the end of 6.6 kV distribution feeders. Therefore, no load is assumed in order to fundamentally investigate the influence of only the PV system.

3. Vector Diagram of Voltage

3.1. Vector Locus of Receiving-End Voltage. In this section, our previous paper [15] is briefly reviewed. Figure 2 illustrates the vector diagram among the receiving-end voltage V_r, sending-end voltage V_s, and the inverse current I from the PV system. Here, the power factor is 1 and the whole length of the line is D. The locus of the voltage vector V_r with an increase in I is indicated by a bold solid line. A circle centered on point "o" and having the sending-end voltage V_s as its radius is drawn by a dashed line.

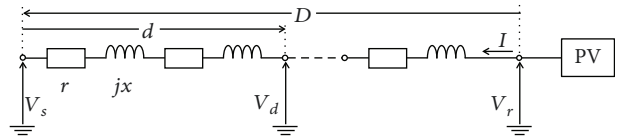

Figure 1: Single-phase equivalent circuit of a power distribution system.

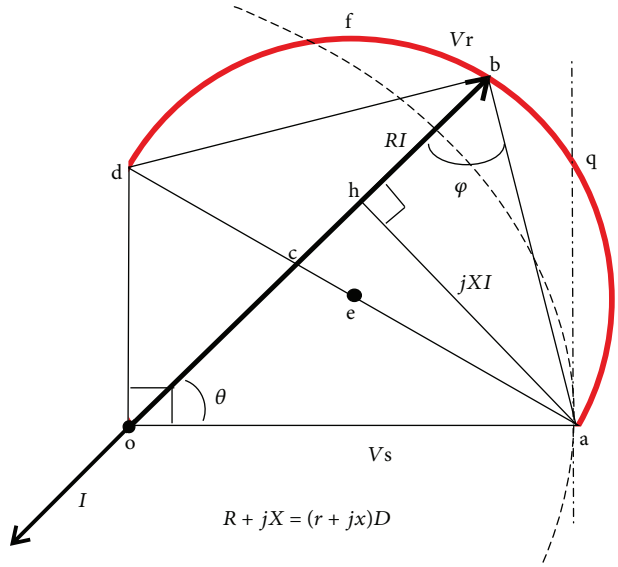

Figure 2: The locus of the receiving-end voltage vector.

The ratio of rDI and xDI is always constant. As the current increases, triangle "abh" consisting of $RI(=rDI)$ and $XI(=xDI)$ becomes similarly large. Triangle "abh" represents the magnitude of the voltage rise at the receiving end due to the line impedance and the reverse current I.

In this case, although the current I is in phase with the voltage V_r, the phase of the current I as well as the voltage V_r is advanced compared to the voltage V_s by the angle of θ. As the current increases, the phase angle θ increases and finally becomes $\theta = \pi/2$.

Angle "dba" is always a right angle regardless of the magnitude of the inverse current I. Therefore, the locus of the receiving-end voltage V_r is drawn with a circular arc whose diameter is shown by line "ad."

The tangent line at point "a" to the circle drawn with a dashed line is shown by a one-dot chain line. Point "q" is the intersection point between the bold solid line and the one-dot chain line. The maximum receiving-end voltage V_{r-max} is given by line "oq."

3.2. Expression of the Receiving-End Voltage. From Figure 2, the magnitude of the receiving-end voltage is expressed by the following expression:

$$V_r(I) = rDI + \sqrt{V_s^2 - (xDI)^2}. \quad (1)$$

Using $V_s^2 - (xDI)^2 \geq 0$ due to voltage stability, the allowable range of the current I is deduced as

$$0 \leq I \leq \frac{V_s}{xD}. \quad (2)$$

The allowable limit of the current I is also represented as

$$I_{\max} = \frac{V_s}{xD}. \quad (3)$$

The magnitude of the maximum receiving-end voltage becomes

$$V_{\text{r-max}} = \frac{V_s}{\sin(\varphi)}, \quad (4)$$

where $\tan \varphi = x/r$.

When $V_r = V_s$, the current I is given by the following expression:

$$I = \frac{2rV_s}{z^2 D}, \quad \text{at } V_r = V_s, \quad (5)$$

where $z = \sqrt{r^2 + x^2}$.

From the abovementioned expressions, the following facts are found out:

(1) With an increase in the sending-end voltage V_s, both $I_{\max}$ and $V_{\text{r-max}}$ become large

(2) Thus, even if the receiving-end voltage V_r becomes higher than the allowable voltage range, V_r could fall within the allowable range by decreasing V_s. However, the decrease in V_s might cause the opposite effect to reduce the allowable limit of the current I

(3) $V_{\text{r-max}}$ is independent of D and I but depends only on the line impedance. When the magnitude of the resistance component of the line impedance becomes relatively smaller than that of the reactance component, $V_{\text{r-max}}$ is suppressed to be low

(4) The allowable limit of the current I, $I_{\max}$, is in inverse proportion to the product of D and x, that is, the whole reactance component of the line. $I_{\max}$ is independent of the resistance component

(5) When the whole length or the reactance component of the distribution line becomes larger, the allowable limit of the current I becomes smaller

(6) Thus, the voltage instability is likely to be caused by an increase in D

3.3. A Case Study on the Receiving-End Voltage as a Function of Line Current. As a case study, the dependence of the receiving-end voltage V_r on the line current is calculated for the line impedance of $0.3 + j0.4\,\Omega$/km and a whole line length of 25 km. Figure 3 shows the receiving-end voltage V_r as a function of the line current $I_L = I/\sqrt{3}$. In this figure,

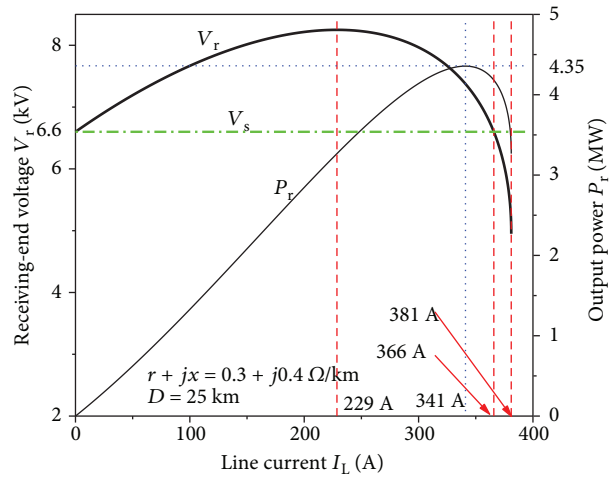

FIGURE 3: Receiving-end voltage as a function of the line current in the case of $r + jx = 0.3 + j0.4\,\Omega$/km and $D = 25$ km.

sending-end voltage $V_s = 6.6$ kV and output power of the PV system, $P_r = V_r I = \sqrt{3} V_r I_L$, are also drawn with a one-dot chain straight line and with a thin solid line, respectively.

In this case, the receiving-end voltage V_r is increased with an increase in the line current until $I_L = 229$ A. After the receiving-end voltage V_r indicates a maximum magnitude at $I_L = 229$ A, the voltage V_r begins to be reduced with an increase of I_L. At $I_L = 366$ A, the magnitude of the voltage V_r becomes the same as that of the sending-end voltage V_s. When the line current increases to more than 366 A, the receiving-end voltage becomes less than the sending-end voltage. The allowable maximum line current is 381 A.

Concerning the output power of the PV system, P_r increases with an increase in the line current until the line current reaches 341 A, where P_r is at its maximum. In the range of $I_L = 229$ A to 341 A, although the receiving-end voltage V_r decreases with an increase in the line current I_L, P_r continues to increase with an increase in the line current I_L because of the small decreasing rate of V_r. When the PV system is controlled to keep the output current constant, the output current from the PV system can be enlarged to larger than 341 A, while the output power must be reduced.

4. Voltage Profile along the Line

4.1. Vector Diagram. Figures 4–8 illustrate the vector diagram of the voltage vector V_d on the line away from the sending end by a distance d.

In Figure 4, triangle "agk" indicates the magnitude of the voltage rise of V_d due to the line impedance. The vector end point of V_d moves on line "ab" with an increase in the distance d because the line impedance is directly proportional to d.

Figure 5 shows the vector diagram where the receiving-end voltage becomes maximum. Line "ab" exists outside of the circle of the one-dot chain line. Therefore, the voltage V_d is always larger than the sending-end voltage, and V_d rises with an increase in d.

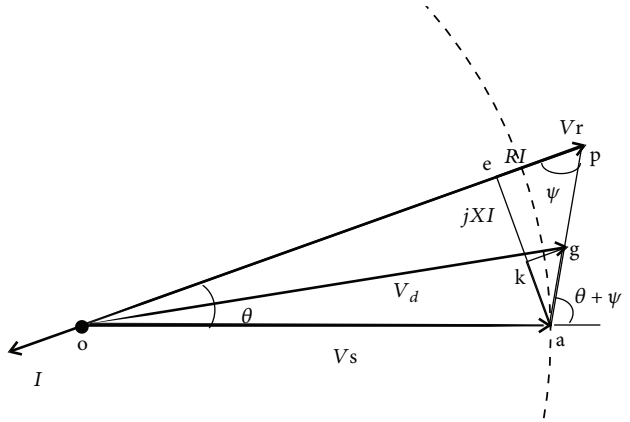

Figure 4: Vector diagram of voltage in the case of a relatively small line current.

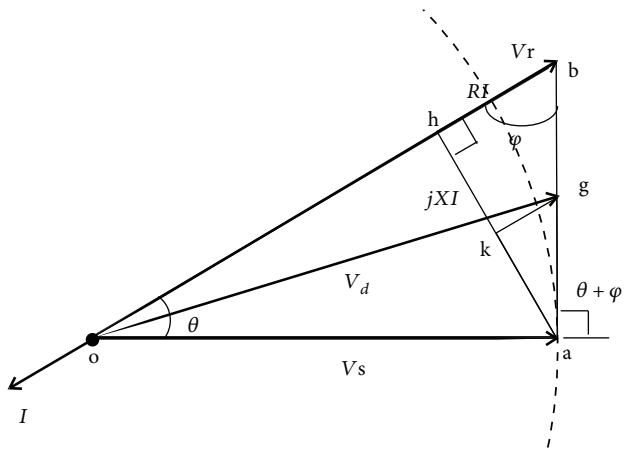

Figure 5: Vector diagram of voltage in the case of the maximum receiving-end voltage.

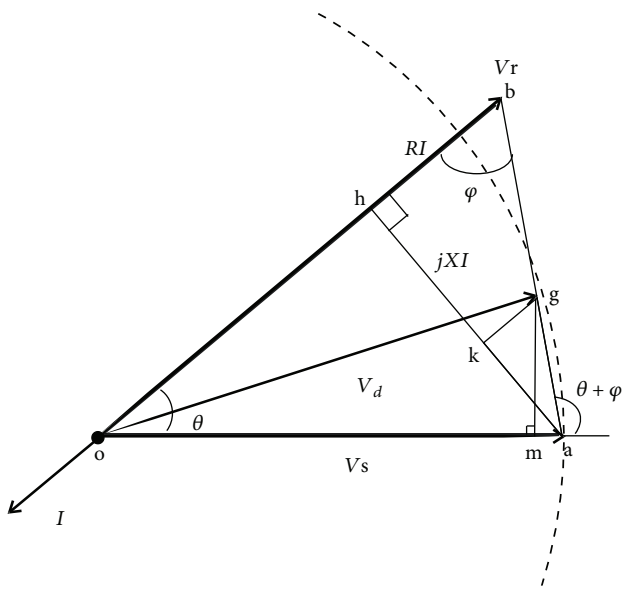

Figure 6: Vector diagram of voltage in the case of a relatively large line current.

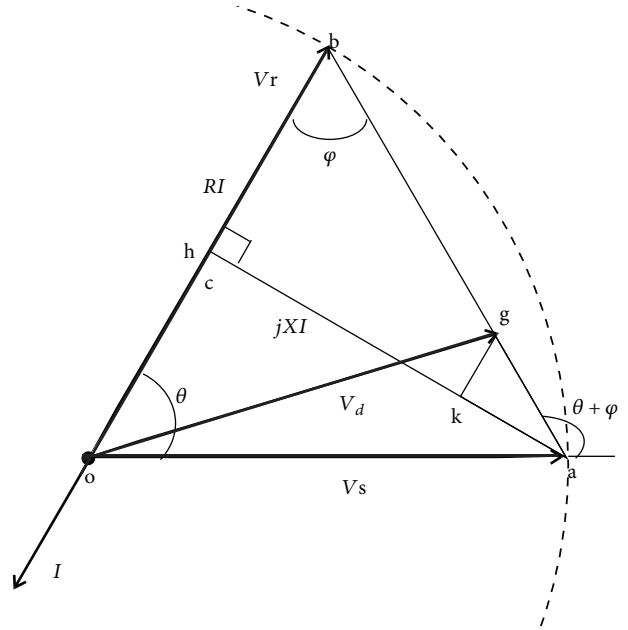

Figure 7: Vector diagram of voltage in the case of $V_r = V_s$.

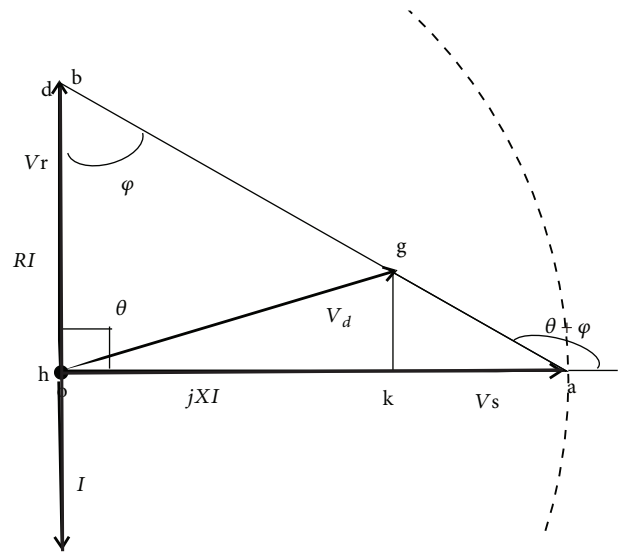

Figure 8: Vector diagram of voltage in the case of the allowable limit of line current.

In the case of Figure 6, line "ab" exists partially in the inner side and the outer side of the one-dot chain line circle. Therefore, the voltage V_d is smaller than V_s near the sending end, whereas V_d is larger than V_s near the receiving end.

On the other hand, Figures 7 and 8 indicate the vector diagram at $V_r = V_s$ and at the allowable limit of the line current, respectively. In these figures, line "ab" is in the inner side of the one-dot chain line circle. Therefore, the voltage V_d is always smaller than the sending-end voltage V_s.

4.2. Expressions of Voltage Profile along the Line. From Figure 6, the voltage V_d at the node far away from the sending end by d is given as follows:

$$V_d = \sqrt{\overline{\mathrm{gm}}^2 + \overline{\mathrm{mo}}^2} = \sqrt{[(zd)I\sin(\lambda)]^2 + [V_s + (zd)I\cos(\lambda)]^2}, \quad (6)$$

where $\lambda = \theta + \varphi$,

$$\sin\theta = \frac{(xD)I}{V_s}. \quad (7)$$

4.3. Dependence of Voltage Profile on Line Current. As a case study, the voltage profile along the power distribution line described in Section 3.2 ($r + jx = 0.3 + j0.4\,\Omega$/km) was estimated as a function of the line current. Figure 9 shows the voltage profiles derived for the line current of 112 A, 229 A, 319 A, 341 A, 366 A, and 381 A. Consequently, the following results were found:

(1) When the line current I_L is 112 A, the voltage V_d increases almost proportionally to d

(2) When I_L becomes 229 A, where the sending-end voltage V_r is at its maximum, the profile of the voltage V_d shows a downward convex waveform. However, the voltage V_d is always higher than the sending-end voltage until the line current is 229 A

(3) When I_L becomes more than 229 A, the voltage V_d strongly shows a similar tendency as stated above so that V_d begins to be lower than 6.6 kV just near the sending end

(4) When I_L is 319 A or 341 A, the profile of the voltage V_d consists of the lower zone near the sending end and higher zone near the receiving end

(5) When I_L reaches 366 A, the voltage at the receiving end coincides with the voltage at the sending end. The voltage V_d is always smaller than the sending-end voltage

(6) When the line current reaches 381 A, which is the allowable limit of the line current, the receiving-end voltage V_r and the voltage V_d are always smaller than the sending-end voltage

(7) In the case of $r + jx = 0.3 + j0.4\,\Omega$/km and $D = 25$ km, the line current at more than 381 A cannot flow safely due to equation (2).

4.4. Dependence of Voltage Profile on Line Length D. In this section, the dependences of the voltage distribution along the line on the whole line length D are discussed for two distribution lines, whose impedances are $0.3 + j0.4$ and $0.15 + j0.4\,\Omega$/km. The latter impedance is one with a wire thicker than that of the former one. In Figure 10, the voltage profiles along the line are illustrated as a parameter of the whole line length D for the line current of 262 A, which corresponds to the output power of 3,000 kW based on the rating voltage of 6.6 kV.

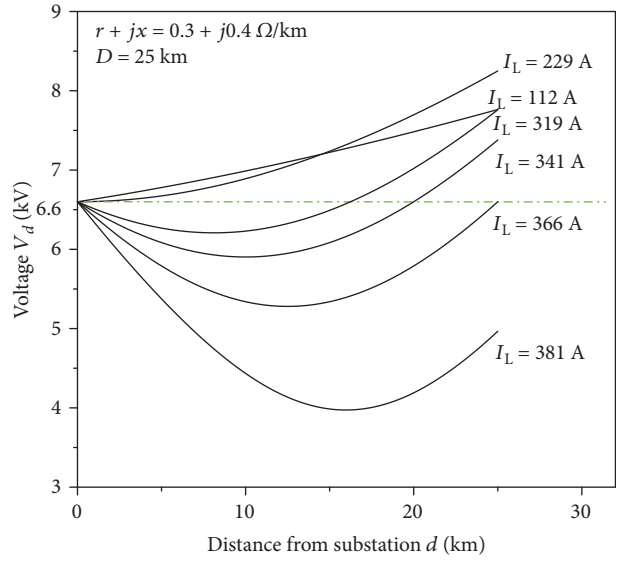

Figure 9: Voltage profiles as a parameter of the line current for the whole line length $D = 25$ km (line impedance of $0.3 + j0.4\,\Omega$/km).

The following results can be pointed out:

(1) In the case of $D = 5$ km, the voltage V_d increases almost proportionally to d

(2) In the case of $D = 10$ km, the profile of the voltage V_d shows a downward convex waveform

(3) When the whole line length D is shorter than 21.8 km for $r + jx = 0.3 + j0.4\,\Omega$/km or 12.8 km for $0.15 + j0.4\,\Omega$/km, where the receiving-end voltage V_r becomes maximum, the voltage V_d is always higher than the sending-end voltage

(4) When D is longer than 21.8 km or 12.8 km, the profile of the voltage V_d consists of the lower zone near the sending end and the higher zone near the receiving end compared with the sending-end voltage

(5) When D reaches 34.5 km or 23.9 km, the voltage at the receiving end coincides with the voltage at the sending end. The voltage V_d is always smaller than the sending-end voltage

(6) When D is larger than 34.5 km or 23.9 km, the receiving-end voltage V_r and the voltage V_d are always smaller than the sending-end voltage

(7) In both cases of $r + jx = 0.3 + j0.4\,\Omega$/km and $0.15 + j0.4\,\Omega$/km, the line current of 262 A cannot flow safely through the power distribution system of which the whole line length D is more than 36.3 km due to equation (2)

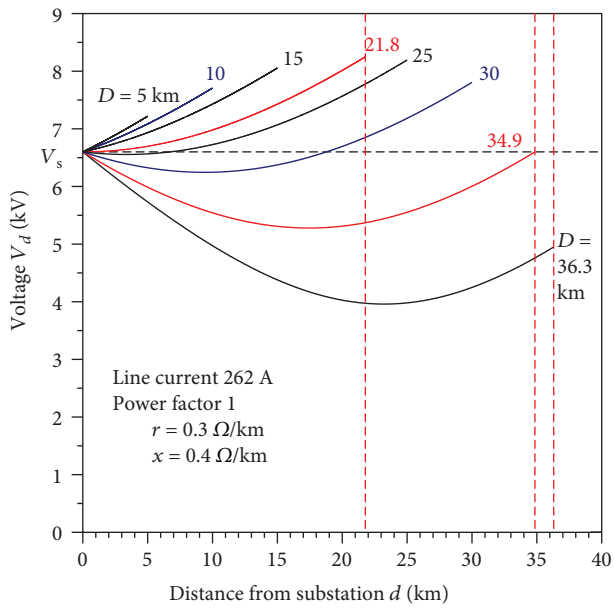

(a) Line impedance of $0.3 + j0.4\,\Omega$/km

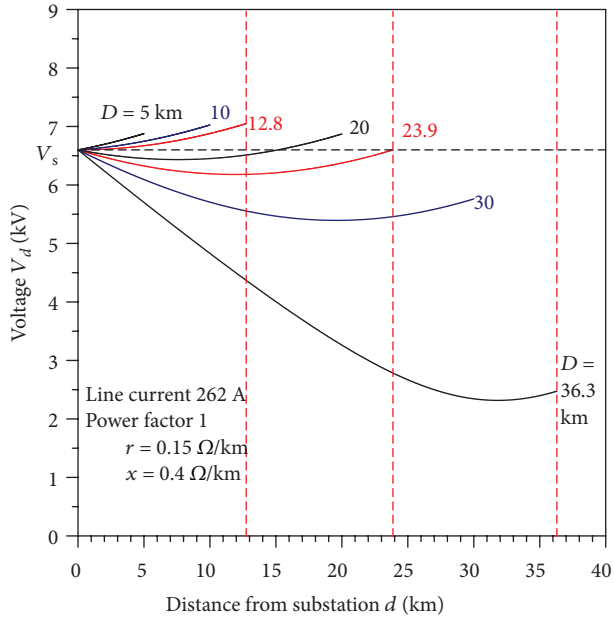

(b) Line impedance of $0.15 + j0.4\,\Omega$/km

FIGURE 10: Dependence of the voltage profile on the whole line length D at a line current of 262 A.

5. Effect of Output Power from PV System

5.1. Voltage Power Characteristics and Allowable Limit of Output Power from the PV System. Figures 2 and 4 give the following expressions:

$$\begin{aligned} (V_r - rDI)^2 + (xDI)^2 &= V_s^2, \\ V_r^2 - 2rDIV_r + (rDI)^2 + (xDI)^2 &= V_s^2. \end{aligned} \tag{8}$$

Using $P_r = V_r I$, equation (8) is reduced as follows:

$$\begin{aligned} V_r^2 - 2RP_r + \left(rD\frac{P_r}{V_r}\right)^2 + \left(xD\frac{P_r}{V_r}\right)^2 &= V_s^2, \\ V_r^4 - \left(2rDP_r + V_s^2\right)V_r^2 + (zD)^2P_r^2 &= 0. \end{aligned} \tag{9}$$

This equation has the following roots:

$$V_r^2 = \frac{\left(2rDP_r + V_s^2\right) + \sqrt{\left(2rDP_r + V_s^2\right)^2 - 4(zD)^2P_r^2}}{2}. \tag{10}$$

Thus, the voltage-power characteristics are represented by the following expression:

$$V_r = \sqrt{\frac{V_s^2 + 2rDP_r + \sqrt{V_s^4 + 4rDV_s^2P_r - 4(xD)^2P_r^2}}{2}}. \tag{11}$$

The real root must exist:

$$V_s^4 + 4rDV_s^2P_r - 4(xD)^2P_r^2 > 0. \tag{12}$$

Consequently, the allowable output power is expressed as follows:

$$0 < P_r < \frac{r + \sqrt{r^2 + x^2}}{2x^2D}V_s^2. \tag{13}$$

This equation suggests the following facts:

(1) The allowable limit of the output power from the PV system is proportional to the square of the sending-end voltage. Thus, the allowable limit can be enlarged by the rise of the sending-end voltage

(2) The allowable limit is inversely proportional to the whole line length D. Therefore, the long power distribution system cannot be allowed to introduce the larger-power PV system compared with the short-line power distribution system

(3) The resistance component of the line impedance becomes the smaller, and the allowable limit of the output power is reduced

5.2. Dependence of Receiving-End Voltage V_r on Output Power P_r from the PV System. The solid line in Figure 11 illustrates the dependence of the receiving-end voltage V_r on the output power P_r derived from equation (13) for the line impedance of $r + jx = 0.3 + j0.4\,\Omega$/km. In this figure, the corresponding line current I_L is also plotted as a function of the output power P_r. The solid lines in this figure show that the maximum magnitudes of P_r and I_L are 4.36 MW and 341 A for $0.3 + j0.4\,\Omega$/km, respectively. In the case of $0.3 + j0.4\,\Omega$/km, V_r is always higher than V_s.

As described in Section 3.3, if the PV system is strongly controlled to keep the line current constant, the line current could be enlarged to more than 341 A by reducing the output

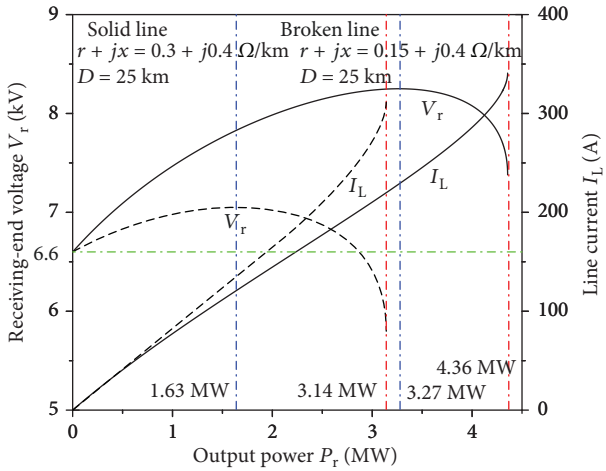

Figure 11: Dependence of the receiving-end voltage V_r on output power P_r for the whole line length $D = 25$ km (line impedances of $0.3 + j0.4\ \Omega$/km and $0.15 + j0.4\ \Omega$/km).

power. However, when the PV system is controlled to keep the output power constant, P_r and I_L are limited to the abovementioned magnitudes.

The dashed lines in Figure 11 shows the ones for $0.15 + j0.4\ \Omega$/km, which is the impedance for the thicker wire compared to the abovementioned wire of $0.3 + j0.4$ W/km. In the case of this line impedance, the maximum magnitudes of P_r and I_L are 3.14 W and 312 A, respectively. These magnitudes are smaller than the ones for $0.3 + j0.4\ \Omega$/km.

It is pointed out that the use of the thicker wire brings about the reduction of the voltage rise, but concurrently the allowable limit of the output power of the PV system must be decreased.

5.3. Dependence of Voltage Profile V_d on Output Power from the PV System P_r. Figures 12(a) and 12(b) show the voltage profiles as a parameter of the output power P_r, the former for $r + jx = 0.3 + j0.4\ \Omega$/km and the latter for $r + jx = 0.15 + j0.4\ \Omega$/km. In Figure 12(a), only four voltage profiles can be seen, which are the same as those of the upper four profiles in Figure 8, because of the allowable range of the output power.

In Figure 12(b), five profiles are drawn. In the case of $0.15 + j0.4\ \Omega$/km, when the output power from the PV system is larger than 2.86 MW, the receiving-end voltage V_r and the voltage V_d are always smaller than the sending-end voltage V_s. However, the allowable limit of the output power is 3.14 MW, which is smaller than that of $0.3 + j0.4\ \Omega$/km. It should be noted that if the thick wire is used as the power distribution line, too much reduction of the voltage might be caused by the large output power of the PV system.

6. Conclusion

The voltage rise and fall characteristics caused by the introduction of large PV systems into a long power distribution system is studied in this work by using vector diagrams of a single-phase equivalent circuit.

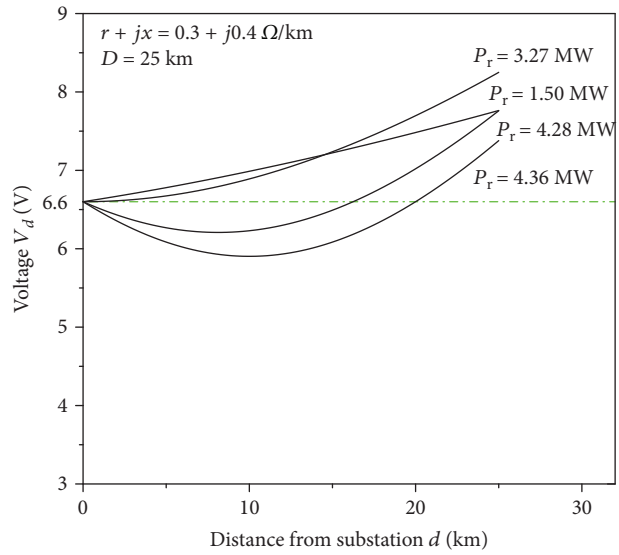

(a) Line impedance of $0.3 + j0.4\ \Omega$/km

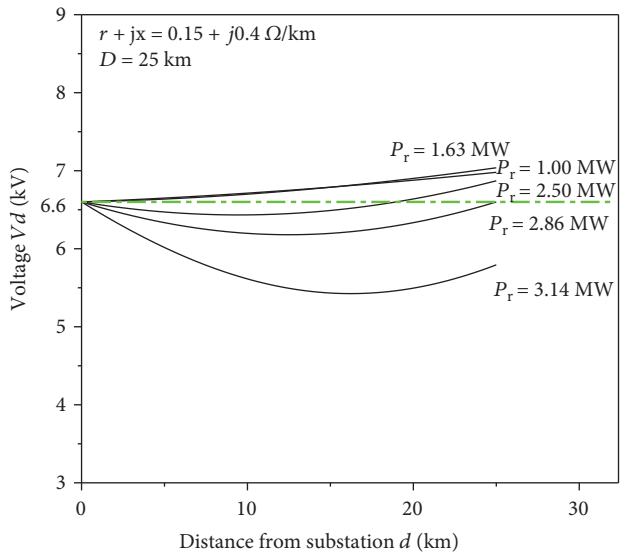

(b) Line impedance of $0.15 + j0.4\ \Omega$/km

Figure 12: Voltage profile V_d as a parameter of output power P_r for the whole line length $D = 25$ km.

When the line current on the circuit is small, the voltage on the line monotonically increases from the sending end to the receiving end. When a relatively large current flows, it causes a voltage reduction near the distribution substation even if no load exists.

The allowable limit of the output power from the PV system can be enlarged by the rise of the sending-end voltage. However, it heightens the receiving-end voltage and the voltage profile. It should be noted that the small resistance component of the line impedance prevents the rise of the voltage and also reduces the allowable limit of the output power.

Data Availability

The data used to support the findings of this study are included within the article.

Conflicts of Interest

The authors declare that there is no conflict of interest regarding the publication of this paper.

References

[1] T. Stetz, M. Kraiczy, and K. Diwold5, "High penetration of PV in local distribution grids," IEA PVPS Task14-2Report, 2014.

[2] dena: dena Ancillary Services Study 2030, "Security and reliability of a power supply with a high percentage of renewable energy. Final report," 2014.

[3] K. Ishikawa, H. Taniguchi, H. Suzuki, Y. Ota, and Y. Mizuno, "Fundamental voltage characteristics in power system with a large penetration of photovoltaic generation," *IEEJ Transactions on Power and Energy*, vol. 134, no. 1, pp. 2–8, 2014.

[4] K. Ishikawa, H. Taniguchi, H. Suzuki, Y. Ota, and Y. Mizuno, "Fundamental study on voltage stability in power system with large penetration of photovoltaic generation considering induction motor dynamics," *IEEJ Transactions on Power and Energy*, vol. 134, no. 7, pp. 568–578, 2014, (in Japanese).

[5] M. Imanaka, M. Machida, J. Baba, and D. Iioka, "Basic study on high penetration of photovoltaics with advanced voltage control and partial voltage boost in distribution networks—1. Analysis of hosting capacity," The Papers of Joint Technical Meeting, PE-16-064/PSE-16-084, IEE Japan, 2016.

[6] C. L. Masters, "Voltage rise: the big issue when connecting embedded generation to long 11 kV overhead lines," *Power Engineering Journal*, vol. 16, no. 1, pp. 5–12, 2002.

[7] K. Turitsyn, P. Sulc, S. Backhaus, and M. Chertkov, "Options for control of reactive power by distributed photovoltaic generators," *Proceedings of the IEEE*, vol. 99, no. 6, pp. 1063–1073, 2011.

[8] P. M. S. Carvalho, P. F. Correia, and L. A. F. Ferreira, "Distributed reactive power generation control for voltage rise mitigation in distribution networks," *IEEE Transactions on Power Systems*, vol. 23, no. 2, pp. 766–772, 2008.

[9] A. Samadi, R. Eriksson, L. Söder, B. G. Rawn, and J. C. Boemer, "Coordinated active power-dependent voltage regulation in distribution grids with PV systems," *IEEE Transactions on Power Delivery*, vol. 29, no. 3, pp. 1454–1464, 2014.

[10] D. Iioka, K. Sakakibara, Y. Yokomizu, T. Matsumura, and N. Izuhara, "Distribution voltage rise at dense photovoltaic generation area and its suppression by SVC," *Electrical Engineering in Japan*, vol. 166, no. 2, pp. 47–53, 2009.

[11] J.-H. Choi and J.-C. Kim, "Advanced voltage regulation method of power distribution systems interconnected with dispersed storage and generation systems," *IEEE Transactions on Power Delivery*, vol. 16, no. 2, pp. 329–334, 2001.

[12] D. Ranamuka, A. P. Agalgaonkar, and K. M. Muttaqi, "Online voltage control in distribution systems with multiple voltage regulating devices," *IEEE Transactions on Sustainable Energy*, vol. 5, no. 2, pp. 617–628, 2014.

[13] D. Iioka, K. Miura, M. Machida et al., "Hosting capacity of large scale PV power station in future distribution networks," in *2017 IEEE Innovative Smart Grid Technologies - Asia (ISGT-Asia)*, pp. 1–6, Auckland, New Zealand, 2017.

[14] S. Kikuchi, M. Machida, J. Tamura et al., "Hosting capacity analysis of many distributed photovoltaic systems in future distribution networks," in *2017 IEEE Innovative Smart Grid Technologies—Asia (ISGT-Asia)*, pp. 1–5, 2017.

[15] T. Matsumura, K. Yukita, Y. Goto et al., "A study on rising and reducing process of receiving-end voltage due to introduction of large PV systems into distribution power system," *IEEJ Transactions on Power and Energy*, vol. 138, no. 1, pp. 23–29, 2018, (in Japanese).